

Subscriber access provided by UNIV OF WISCONSIN - MADISON

Influence of Nanoparticle Morphology on Ion Release and Biological Impact of Nickel Manganese Cobalt Oxide (NMC) Complex Oxide Nanomaterials

Mimi Ngoc Hang, Natalie V. Hudson-Smith, Peter L. Clement, Yongqian Zhang, Chenyu Wang, Christy L. Haynes, and Robert J Hamers

ACS Appl. Nano Mater., Just Accepted Manuscript • DOI: 10.1021/acsanm.8b00187 • Publication Date (Web): 02 Apr 2018

Downloaded from http://pubs.acs.org on April 2, 2018

Just Accepted

"Just Accepted" manuscripts have been peer-reviewed and accepted for publication. They are posted online prior to technical editing, formatting for publication and author proofing. The American Chemical Society provides "Just Accepted" as a service to the research community to expedite the dissemination of scientific material as soon as possible after acceptance. "Just Accepted" manuscripts appear in full in PDF format accompanied by an HTML abstract. "Just Accepted" manuscripts have been fully peer reviewed, but should not be considered the official version of record. They are citable by the Digital Object Identifier (DOI®). "Just Accepted" is an optional service offered to authors. Therefore, the "Just Accepted" Web site may not include all articles that will be published in the journal. After a manuscript is technically edited and formatted, it will be removed from the "Just Accepted" Web site and published as an ASAP article. Note that technical editing may introduce minor changes to the manuscript text and/or graphics which could affect content, and all legal disclaimers and ethical guidelines that apply to the journal pertain. ACS cannot be held responsible for errors or consequences arising from the use of information contained in these "Just Accepted" manuscripts.



Influence of Nanoparticle Morphology on Ion Release and Biological Impact of Nickel Manganese Cobalt Oxide (NMC) Complex Oxide Nanomaterials

Mimi N. Hang † , Natalie V. Hudson-Smith $^{\S^{\sharp}}$, Peter L. Clement § , Yongqian Zhang † , Chenyu Wang † , Christy L. Haynes § , Robert J. Hamers † *

[†]Department of Chemistry, University of Wisconsin-Madison, 1101 University

Avenue, Madison, WI 53706, United States

§Department of Chemistry, University of Minnesota, 207 Pleasant Street SE,
Minneapolis, MN 55455, United States

Keywords: Nanomaterial; environmental impact; energy storage; nickel manganese cobalt oxide; cathode materials; toxicity; environmental impact

ABSTRACT: Lithium intercalation compounds such as nickel manganese cobalt oxides, ($Li_xNi_yMn_zCo_{1-y-z}O_2$, 0 < x,y,z < 1, or NMCs) are complex transition metal

[‡]These authors contributed equally to the work

^{*}Corresponding author: rjhamers@wisc.edu

oxides of increasing interest in nanoscale form for applications in electrochemical energy storage and as tunable catalysts. These materials exhibit sheet-like structures that expose low-energy basal planes and higher-energy edge planes in relative amounts that vary with the nanoparticle morphology. Yet there is little understanding of how differences in nanoparticle morphology and exposed crystal planes affects the biological impact of this class of technologically relevant nanomaterials. We investigated how changing nanoparticle morphology from twodimensional (001)-oriented nanosheets to three-dimensional nanoblocks affects the release of ions and the resulting biological impact using Shewanella oneidensis MR-1 as a model organism. NMC nanoparticles were synthesized in sheet-like morphology and then converted to block morphologies by heating, leading to two morphologies of identical chemical composition that were compared to a commercially available NMC. Ion dissolution studies reveal that NMC nanomaterials release transition metal ions incongruently (Ni>Co>Mn) in amounts that vary with nanoparticle morphology. However, when normalized by the specific surface areas, the rates of release of each transition metal from flakes, blocks, and commercial material were equivalent. Similarly, the impact on *S. oneidensis* MR-1 was different when using mass-based dosing, but was nearly identical using surface area-normalized exposure dosing. Our results show that even though nanosheets and nanoblocks expose different crystal faces with significantly different surface energies, the rate of ion release is independent of the distribution of crystal faces exposed and depends only on the total surface area exposed. These data suggest that the key protonation steps that control release of transition metals do not depend on the degree of

coordination of the initially exposed surface, providing insights into the molecularlevel factors that influence environmental impact of complex metal oxide nanomaterials. Our results have significant implications for establishment of methodologies for assessing toxicity of reactive nanomaterials.

1. Introduction

Many emerging nanomaterials of technological relevance are comprised of reactive compositions in which chemical transformations of the materials in aqueous media control their biological interactions and environmental impact. 1-6 Lithium intercalation compounds of the general formula LiMO₂ (where M= transition metal) represent a particularly important class of materials due to their widespread use as energy storage materials in lithium ion batteries⁷⁻¹⁰ and their novel catalytic properties. $^{11-13}$ While lithium cobalt oxide (Li_xCoO_2 , 0 < x < 1, or LCO) has been the material most frequently used cathode for mobile electronics, a desire for increased performance with reduced cost is leading to adoption of various more complex oxides such as lithium nickel manganese cobalt oxide (Li_xNi_yMn_zCo_{1-y-z}O₂, 0 < x,y,z <1, referred to here as "NMC"). 14-17 Like LCO, NMC compounds consist of layers of MO_2 (where M = Ni, Co, Ni in the appropriate stoichiometry) alternating with layers of lithium ions. 18-19 While present-generation commercial NMC materials typically consist of primary particles ~200-1000 nm in size that are sintered into larger aggregates, nanoparticles are formed in situ as a result of mechanical stresses during battery cycling^{5, 20-21} Furthermore, metal oxides of NMC and other compositions have been shown to have improved performance.²²⁻²⁴ The

large-scale use of NMC (up to 100 kg per electric vehicle) increases the potential for environmental release and exposure due, for example, to improper disposal.²⁵⁻²⁷ The incorporation of Ni and Mn to reduce cost also reduces the economic incentives for recycling at end of life²⁸ and leads to increased potential for improper disposal and environmental release. The widespread use and potential environmental impact of NMC makes this class of materials an ideal model system for understanding the factors that control environmental impact of reactive engineered nanomaterials.

A particularly acute challenge in assessing the environmental impact of reactive nanomaterials such as NMC is understanding to what extent their chemical transformation processes are controlled by crystal structure and/or surface properties, and the associated implications for assessing and ultimately predicting the biological impact of nanomaterials.²⁹⁻³² Since NMC have sheet-like crystal structures, their chemical reactivity might logically be expected to depend significantly on the specific crystal faces exposed. 12, 33-35 Prior studies of LiCoO₂ reported that the basal (001) plane has the lowest energy ³⁴ and is least reactive toward the oxygen evolution reaction, 12 while the (104) (012) and (1 $\bar{1}$ 0) surfaces have energies that are slightly higher³⁴ and are more catalytically active.¹² The free energies of the surfaces depend on the oxygen and lithium chemical potentials during synthesis. As a consequence, the morphology and amount of edge- vs. basalplane can be controllably varied. Figure 1 illustrates how the shape of NMC particles changes with different amounts of the (001), (012), and (104) planes exposed. These crystal planes expose transition metals (TMs) and 0 atoms with differing degrees of under-coordination. TMs exposed at the (001) surface are fully

coordinated while those at the (104), (012), and ($1\overline{1}0$) are under-coordinated; 0 atoms are under-coordinated at all surfaces. In aqueous systems the undercoordinated O and TM atoms can interact with water to produce exposed TM-OH groups.^{12, 36-38} In a previous study, we showed that dissolution of transition metals from NMC occurred incongruently in the order Ni>Co>Mn demonstrating that the dissolution processes are *element-specific* within a single nanomaterial. ⁵⁻⁶ Computational studies further support the experimental finding that this dissolution is preferential, nonstoichiometric, and leaves behind transformed particles that are Mn-enriched. ³⁹ We also found that the biological impact of NMC, as assessed through toxicity studies using the Gram-negative bacterium, Shewanella oneidensis MR-1 arose from dissolution of the NMC and the release of transition metal ions, with no observable direct interaction between the nanomaterials and the bacterial cells.⁵⁻⁶ The face-dependent differences in surface energy and degree of transition metal coordination suggest that the atomic structure of NMC surfaces might play an important role in controlling dissolution processes and the release of metals into aqueous matrices. Specifically, dissolution might be expected to be faster at the (104) and (012) faces compared to the (001) basal plane due to the differences in coordination of the exposed transition metals.

Here, we report an investigation of the influence of NMC nanoparticle morphology and the associated distribution of crystal faces on the dissolution and toxicity, using the NMC composition with nominally equal amounts of all three transition metals, Li_xNi_{1/3}Mn_{1/3}Co_{1/3}O₂. While many organisms can be used for toxicity assessment, here we use the bacterium Shewanella oneidensis MR-1 as a model organism due to its global distribution and important role in cycling of metals in the environment, and the fact that it lies at the base of the food chain for many higher organisms.^{32, 40-} ⁴⁵ S. oneidensis is a relatively hearty bacterium, such that toxicity in this species is a strong indicator of toxicity in other species as well. Consequently, S. oneidensis is widely accepted as a model bacterium for investigating metal-induced toxicity in the environment. 5-6, 32, 41-46 We applied synthesis methods that yield two different NMC nanoparticle morphologies: 2-dimensional nanosheets and 3-dimensional nanoblocks, starting from the same starting metal hydroxide intermediates to ensure identical chemical compositions. We then compared the ion release profiles and the biological impact of each morphology, as well as a commercially available

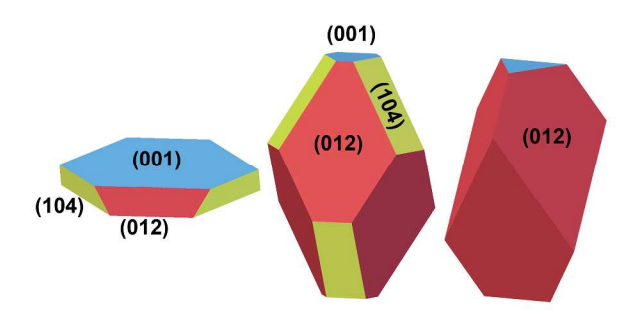


Figure 1. NMC nanoparticle morphology associated with different distributions of low-energy crystal planes. Different families of planes are color-coded for clarity.

NMC, using respirometry and viability measurements of *S. oneidensis* MR-1. By comparing the biological impact as a function of mass-based concentration and as a function of exposed surface area, we establish that the surface area, and not the mass concentration, is the critical variable controlling ion release and toxicity. Our work also implies that while there are significant differences in surface energies of different exposed crystal faces and differences in crystallinity among the materials evaluated, these differences appear to be less important. The present work provides new insights into the relationships between atomic-level structure and subsequent processes that control environmental impact of this emerging class of materials and has implications for best practices in assessing and predicting biological impact of reactive nanomaterials.

2. Experimental Details

2.1 NMC synthesis. Synthesis of nanosheets and nanoblocks of NMC. NMC nanosheets were synthesized using a two-step procedure described previously. 5-6, 47 In this procedure, a nickel manganese cobalt hydroxide precursor was first synthesized via a co-precipitation technique in which an aqueous mixture of 0.1 M nickel (II) acetate, 0.1 M cobalt (II) acetate, and 0.1 M manganese (II) acetate was added dropwise to 0.1 M LiOH under magnetic stirring. A dark brown precipitate of metal hydroxides was collected via repeated cycles of centrifugation (Thermo Scientific Sorvall Legend X1R Centrifuge with Thermo TX-400 rotor, 4696xg) and resuspension in water (1X) and methanol (4X) followed by drying under a flow of nitrogen (g). This metal hydroxide precursor (~250 mg) was then added to a 10 g molten flux under magnetic stirring containing 6:4 molar ratio of LiNO3:LiOH at 205

°C in a poly(tetrafluorethylene) container. The reaction was guenched after 1 h using ultrapure water, producing NMC in a 2-dimensional nanosheet morphology. These nanosheets were isolated using repetitive cycles of centrifugation and resuspension in water (2X) and methanol (3X) and dried. These cleaned nanosheets were then used in the ion release and toxicity measurements described below. To make NMC nanoblocks, the cleaned nanosheets were introduced into a LiNO₃:LiOH (6:4 molar ratio) flux at 600 °C in a platinum crucible in a box furnace. After 4.5 h, the molten salt flux was *very carefully* quenched by quickly pouring directly into ultrapure water in a poly(tetrafluorethylene) beaker, using aluminum foil shielding at the opening to prevent splattering during transfer. The precipitate was then cleaned using centrifugation and resuspension in water (2X) and methanol (3X) and dried, producing NMC nanoblocks. Ultrapure water (18 M Ω •cm resistivity) was used in all experiments; all other reagents were purchased from Sigma Aldrich and used without further purification. We also performed experiments using a commercial battery-grade LiNi_{0.33}Mn_{0.33} Co_{0.33} O₂ material purchased from Electrodes and More, Inc.

- **2.2 Powder X-ray Diffraction (XRD).** To analyze the crystal phase of NMC materials, the Bruker D8 Advance Powder X-ray Diffractometer with a Cu K α source was used. The NMC powder was deposited onto SiO₂ zero diffraction plate (MTI Corp) and smoothed out with a spatula before analysis.
- 2.3 Characterization of NMC stoichiometry and ion release into growth medium. To analyze the chemical composition of both synthesized NMC nanosheets and nanoblocks as well as the commercial material, a Perkin Elmer 4300 Dual View

Inductively Coupled Plasma Optical Emission Spectrometer (ICP-OES) was used. Immediately prior to analysis, materials were separately dissolved in freshly made aqua regia (3:1 v/v mixture consisting of 37% v/v HCl and 70% v/v HNO₃). After 2 h, the dissolved contents were diluted with ultrapure water and analyzed. The standards and water blank were also acidified in a similar manner to the samples to reduce matrix effects; additionally, the standards were prepared using certified reference materials from Sigma Aldrich. The ion concentrations were measured using three analytical replicates.

To characterize the ion release profile each NMC type, suspensions of NMC nanoparticles were magnetically stirred in bacterial growth medium containing 11.6 mM NaCl, 4.0 mM KCl, 1.4 M MgCl₂, 2.8 mM Na₂SO₄, 2.8 mM NH₄Cl, 88.1 μ M Na₂HPO₄, 50.5 μ M CaCl₂, 10 mM HEPES, and 100 mM sodium lactate. The dispersions were maintained at 30 °C in a water bath to mimic bacterial exposure conditions, and aliquots were removed periodically over 72 h and centrifuged at 4696×g for 30 minutes before analysis. The top of the supernatants were then further ultracentrifuged using a Beckman Coulter Optima Ultracentrifuge with a SW-41 Ti Rotor at 288,000×g for 2 h to remove any remaining particles. Only the top half of the supernatant was removed for analysis. To verify effective sedimentation, dynamic light scattering (Malvern Zetasizer Nano ZS) was used. The supernatants were then measured via ICP-OES, with all samples having triplicate analytical and sample measurements.

2.4 Morphology characterization using scanning electron microscopy (SEM).To characterize the morphology of the NMC nanosheets, nanoblocks, and

commercial NMC particles, a methanolic solution of each NMC was made and drop-casted onto boron-doped Si wafers. For imaging, a Leo Supra55 VP scanning electron microscope (SEM) was used with a standard in-lens detector (1 kV incident electron energy).

2.5 Transmission electron microscopy (TEM). Samples were prepared for transmission at a concentration of 0.5 mg/ml and bath sonication for 10 minutes. A drop of the particle dispersion (\sim 6 μ L) was deposited on a 200 mesh copper TEM grid with Formvar and carbon supports (Ted Pella, Inc. Redding, CA) held with reverse grip tweezers and allowed to air dry. TEM micrographs were acquired on a Tecnai T12 transmission electron microscope with an operating voltage of 120 kV.

For time-series TEM to examine the overall nanoparticle change as a function of time, a 50 mg/L dispersion of nanoblocks was prepared in bacterial growth and magnetically stirred at 250 rpm. At each time point (t = 0, 1, 2, 6, 24 h), a 1 mL aliquot of the dispersion was removed. Of this 1 mL aliquot, 6 μ L was deposited on a 200 mesh copper TEM grid with Formvar and carbon supports held with reverse grip tweezers and allowed to air dry.

2.6 Surface area measurements. The Brunauer-Emmet-Teller (BET) specific surface areas of NMC nanosheets and nanoblocks were determined from N_2 adsorption/desorption isotherms obtained using a Micromeritics Gemini VII 2390 Surface Area Analyzer. Each sample holder (Micromeritics) was loaded with $\sim \! 50$ mg of powder and outgassed at 120 °C under vacuum for 1 h using a Micromeritics VacPrep 061 Sample Degas System. The sample was subsequently introduced into

the Surface Area Analyzer and measured over the relative pressure range (P/P_0) of 0.05 to 0.3, where P_0 is the saturated pressure of N_2 .

2.7 Bacterial respiration measurements. The impact of NMC nanosheets and nanoblocks, as well as the commercial NMC, on S. oneidensis MR-1 growth and respiration was assessed by measuring O₂ consumption over time in a 24-vessel respirometry system (Respirometer Systems and Applications, Inc., Springdale, AR.). S. oneidensis MR-1 suspensions in bacterial minimal growth medium were prepared from colonies grown on a Luria-Bertani (LB) agar plate overnight at 30°C and diluted 1:10 v/v;100 mL of this suspension was transferred to 125 mL respirometry vessels fitted with rubber septa. For 5 mg/L exposures, NMC materials were prepared in at 2000mg/L concentration, bath sonicated (Branson 1800 Single Frequency Bath Sonicator, 40 kHz) for 10 minutes, and added to three replicate vessels to achieve the desired concentration. This process was repeated for 50 mg/L doses but initial stocks of NMC material were prepared at 5000 mg/L. Ion control stocks were prepared from NiCl₂, CoCl₂, MnSO₄, and LiOH salts and added to three replicate vessels to achieve ion concentrations matching those of the dissolution studies performed on the NMC nanoparticles. Bacterial suspensions were magnetically stirred at 500 rpm, and oxygen consumption was monitored up to 72 h. Doses of 50 mg/L and 5 mg/L were used in respiration studies based on prior studies indicating that these concentrations produced statistically signficiant changes in respiration. 5 Complementary measurements using Grow-based Viability assay (vide infra) were performed over a wider range of concentrations to ensure that measurements spanned the important range of concentrations.

2.8 Bacterial Growth-based Viability (GBV) Measurements. Colonies of *S. oneidensis* MR-1 were grown on LB agar plates overnight at 30 °C, and then transferred into 10 mL of LB broth. This inoculate was incubated in an orbital shaker (300 RPM, 30 °C) until bacteria reached the mid-log phase (OD₆₀₀ = 0.3-0.6), approximately 4 hours. Bacteria were pelleted by centrifugation at 750×g, and the LB supernatant was removed. Bacteria were resuspended in 0.85% NaCl solution, washed by centrifugation at 750×g, and then suspended in a growth medium consisting of 11.6 mM NaCl, 4.0 mM KCl, 1.4 M MgCl₂, 2.8 mM Na₂SO₄, 2.8 mM NH₄Cl, 88.1 μ M Na₂HPO₄, 50.5 μ M CaCl₂, 10 mM HEPES, and 100 mM sodium lactate. We refer to medium having composition as "minimal growth medium". The optical density of this solution was adjusted to 0.1.

A growth-based viability assay was then used to establish the viability of populations after exposure to nanomaterials, as described previously. As Briefly, the OD600 = 0.1 solution of *S. oneidensis* MR-1 was considered as a negative control with 100% viability. We refer to this as "100% viability stock." A calibration curve was built by serially diluting (1:1) the 100% viability stock to 50, 25, 12.5, and 6.25% viable. Separately, for each nanoparticle exposure, a 180 μ L aliquot of the 100% viability stock was treated with 20 μ L of nanoparticle dispersion to achieve the desired dose or water for the negative control. After a 3 h exposure, 5 μ L of each suspension was transferred to wells containing 195 μ L of LB broth in a 96-well plate. This 96-well plate was transferred to a Biotek Synergy 2 plate reader at 30 °C, and the OD600 was measured every 20 minutes after 30 seconds of shaking to obtain growth curves. Processing of data was achieved using RStudio as described

previously.⁴⁸ For the nanoscale NMC materials, both sheets and blocks, settling was not observed in the time required to prepare dilutions of doses. However, commercial materials settle quickly (within seconds to a minute) and were resuspended as needed agitation in order to prepare a proper series of doses. GBV measurements were performed at concentrations of 100, 50, 25, 12.5, 6 mg/L for nanosheets and nanoblocks and 1000, 500, 250, 125, and 60 ppm for commercial NMC, spanning the range of concentrations where toxic effects are observed.

3. Results and Discussion

3.1 Characterization of nanoscale NMC. ICP-OES analysis of the acid-digested nanosheets show that [Li]/[Ni] = (2.32 ± 0.01) , [Ni]/[Mn] = (0.99 ± 0.03) , and [Ni]/[Co] = (0.94 ± 0.02) , indicating that the material contains stoichiometric amounts of Ni:Mn:Co, with the material being ~75 % lithiated. A similar analysis of the acid-digested nanoblocks show that [Li]/[Ni] = (2.80 ± 0.04) , [Ni]/[Mn] = (0.97 ± 0.02) , and [Ni]/[Co] = (0.99 ± 0.10) , indicating that the Ni:Mn:Co ratios stay the same after high temperature treatment with the material being ~92 % lithiated. In summary, the nanosheets and nanoblocks may be thought of as Li_{0.75}Ni_{0.32}Mn_{0.33}Co_{0.35}O₂ and Li_{0.92}Ni_{0.33}Mn_{0.34}Co_{0.33}O₂, respectively.

Figure 2a, b, and c show SEM images of synthesized NMC nanosheets and nanoblocks and of a commercial battery-grade NMC material. The SEM images were selected to show a large field-of-view to represent the overall shapes of the particles. Moreover, clustered regions were selected to show particles situated at different angles as they dried after drop-casting onto a Si substrate. Figure 2a shows that the majority of NMC nanosheets lie with their basal (001) plane exposed

upward, revealing nanosheets sheets with rounded hexagonal corners, SEM images show typical basal plane widths of ~ 70 nm; TEM images of similar NMC nanosheets show that the individual sheets are <5 nm in thickness. In Figure 2b, upon postsynthetic treatment in a molten Li salt flux at 600 °C, the nanosheets have transformed into 3-dimensional particles that we refer to as nanoblocks. Additional TEM analysis further shows that these are 3-dimensional and have block-like shapes that are frequently slightly elongated. We analyzed the dimensions of 155 particles (as projected onto the TEM imaging plane) and found the longest dimension = 47 ±15 nm and shortest dimension=33 ± 11 nm, for an aspect ratio (longest dimension divided by shortest dimension) of 1.5 ± 0.3 . While high-resolution images do not reveal obvious facets that would allow us to identify a preponderance of specific crystal planes, nanoparticles with significant amounts of exposed (104) planes should be slightly elongated as depicted in Fig. 1, with a maximum aspect ratio of 2.5. The nanosheets in Fig. 2a expose almost entirely the NMC basal plane, while the nanoblocks (Fig. 2b) and commercial NMC (Fig. 2c) expose additional crystal faces. Our results are consistent with prior studies of LiCoO₂ showing that there are several planes with similar free energies.³⁴

Additional experiments were performed to investigate how the molten salt flux

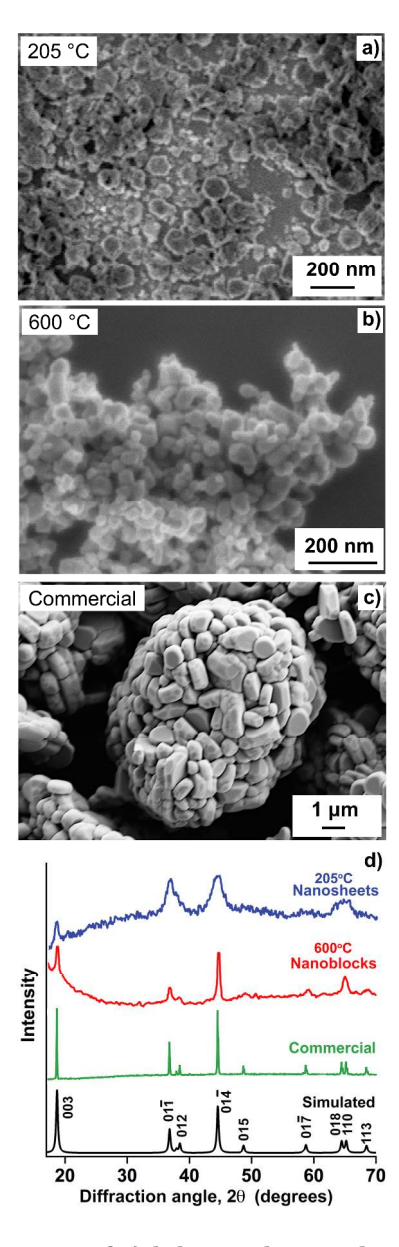


Figure 2. SEM images of a) lab-synthesized NMC nanosheets, b) lab-synthesized NMC nanoblocks, and c) commercial NMC particles. Panel d) shows x-ray diffraction data from each sample along with a simulated spectrum including broadening for a 25 nm diameter nanoparticles.

temperature influenced particle morphology. SEM images obtained at temperatures between 300 and 500 °C (Supporting Information, Figure S1) show that the individual particles undergo morphological transformations, and that even at 500 °C, there are still some flakes that have not transformed into blocks, while at 600 °C all particles have transformed. Additional measurements at different times (Figure S2a-c) show that nanoparticle morphology does not change significantly as a function of processing time in the molten salt flux for times between 1 hour and 4.5 hours.

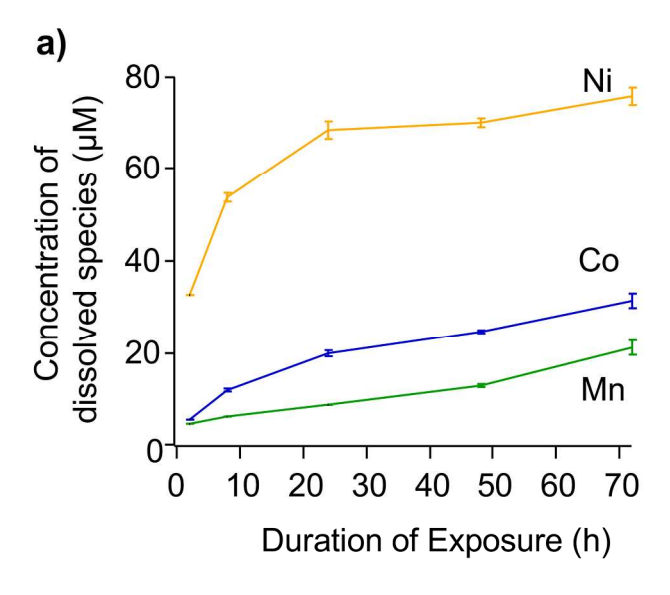
Figure 2d shows X-ray diffraction patterns for NMC nanoblocks, nanosheets, and commercial NMC particles. XRD patterns for nanosheets and nanoblocks were smoothed to 0.25° resolution using a median filter to reduce noise; no other background subtraction was performed. Also shown is a simulated spectrum based on the published lattice parameters,⁴⁹ including broadening appropriate to a 25 nm nanoparticle.⁵⁰ All three materials exhibit diffraction peaks corresponding to the R3m space group reported previously for NMC, 14, 51 with no evidence for additional peaks. The peak broadening for nanoblocks and nanosheets arises both from the small size of the nanoparticles and from residual disorder. Nanoblocks formed at higher temperature show sharper reflections compared to the nanosheets, indicating that the higher temperature synthesis may have increased order in the material. Finally, the nanosheets and nanoblocks show a reduced intensity of the (003) reflection compared to the (104) reflection.⁵²⁻⁵³ This suggests that there is some cation disorder in the lattice, likely from some Ni²⁺ ions located at Li⁺ sites, as discussed later.

Table 1. Ratio of total concentration of transition metals released from nanosheets and nanoblocks at 50 mg/L mass concentration after 72 h, and comparison with ratio of BET surface areas.

| C _{nanosheets} / C _{nanoblocks} | | | | Ratio via BET |
|---|-----------|-----------|--------------|---------------|
| Ni | Mn | Со | Ni + Mn + Co | surface areas |
| 3.9 ± 0.2 | 8.0 ± 0.7 | 3.5 ± 0.3 | 4.1 ± 0.2 | 5.2 ± 0.1 |

3.2 Impact of morphology on release of ions. To characterize how the different morphologies of NMC impact material transformation in bacterial growth medium, ion release profiles were measured for each morphology over 72 h. Figures 3a-c show the concentration of ions released in growth medium as a function of time after introduction of 50 mg/L of NMC nanosheets, nanoblocks, or commercial NMC, respectively. For all three NMC samples, the ions are released incongruently following the trend Ni>Co>Mn. A comparison of the two nanoscale morphologies shows that for equivalent mass concentrations, NMC nanoblocks release less transition metals as compared to nanosheets of NMC or to commercial material. While the release of transition metals is of greatest concern from a biological impact standpoint, Figure S3 in the SI shows that Li release occurs quickly and is the ion released at the highest levels in all cases.

To account for differences in surface area between the lab-synthesized nanosheets, lab-synthesized nanoblocks, and commercial NMC, BET surface areas (SA) of each material were measured. These measurements yielded values of 127.2 \pm 0.4 m²/g for nanosheets, 24.32 \pm 0.15 m²/g for nanoblocks, and 0.98 \pm 0.07 m²/g



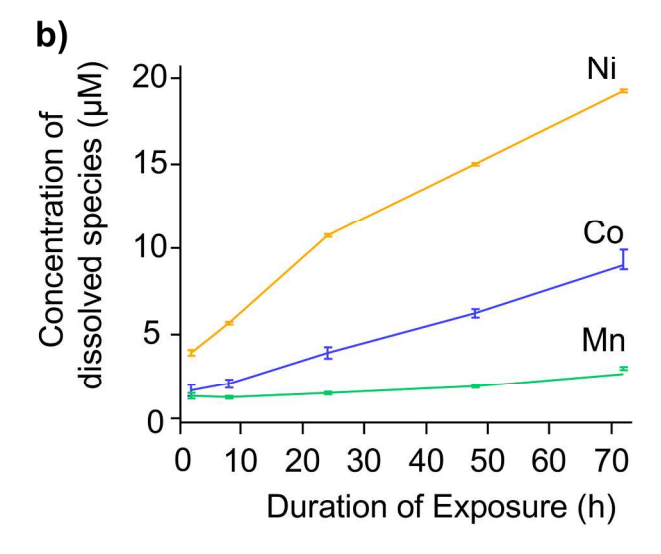


Figure 3. Transition metal ion release profiles in bacterial growth medium of a) NMC nanosheets and b) NMC nanoblocks.

for the commercial NMC material. Thus, for equivalent masses, nanosheets and nanoblocks have relative surfaces areas of $SA_{nanosheets}/SA_{nanoblocks} = 5.3 \pm 0.4$ and $SA_{nanosheets}/SA_{commercial} = 130 \pm 9$. Table 1 shows the ratio of ion concentrations produced from nanosheets and nanoblocks for each transition metal ion. These data show the ratio of concentration of released transition metal ions (4.1 ± 0.2) is close to the ratio of total surface areas (5.3 ± 0.4) .

3.3 Impact of morphology on *Shewanella oneidensis MR-1.* To analyze how the

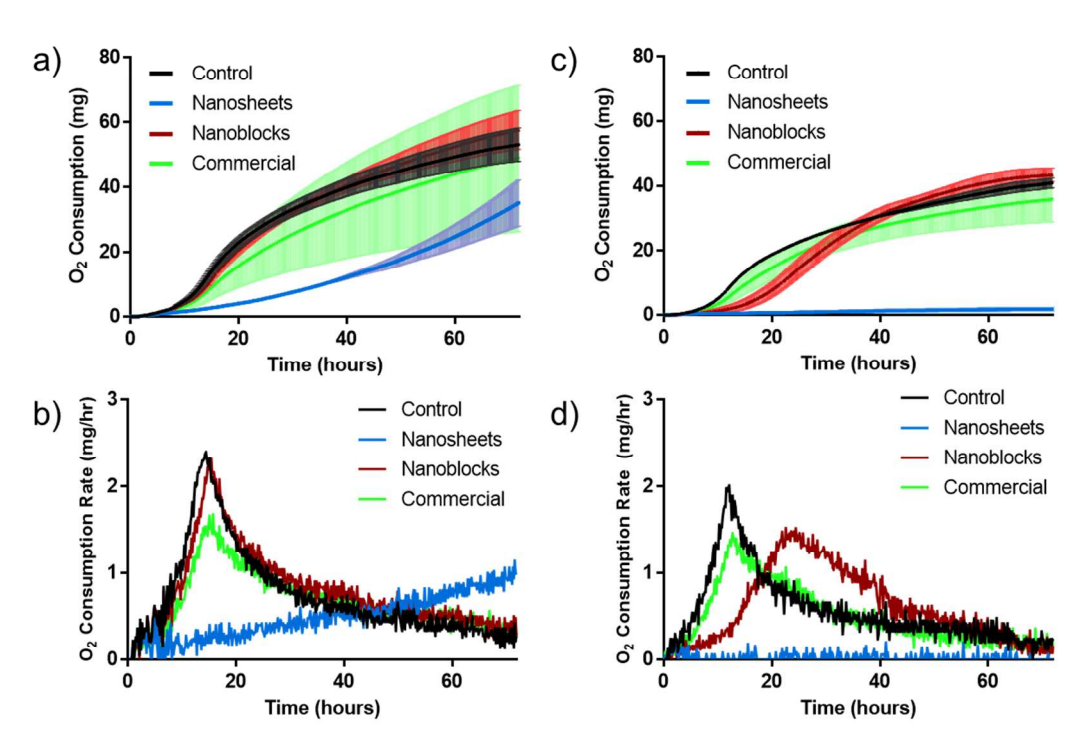


Figure 4. Respirometry traces for a) 5 mg/L dose of each morphology b) first derivative of the 5 mg/L dose c) 50 mg/L dose of each morphology d) first derivative of the 50 mg/L dose. Black trace, control. Blue trace, nanosheets, Red trace, nanoblocks. Green trace, commercial NMC. Error bars represent standard error of the mean from replicate measurements.

differences in NMC morphology and presented crystal faces impact growth and survival of S. oneidensis MR-1, we monitored bacterial aerobic respiration over the course of 72 h exposures. During exposure, stirring was used to encourage interaction between the nanoparticles and bacteria. However, no attempt was made to control particle aggregation state because nanoparticle aggregation is expected to occur under environmentally relevant conditions and can depend on many variables. Fig. 4 shows the raw respirometry data (Fig. 4a, 4c) and the first derivative (Fig. 4b, 4d) obtained used NMC concentrations of 5 mg/L (Fig. 4a, 4b) and 50 mg/L (Fig. 4c, 4d) along with controls in which no NMC was added. In the absence of any NMC, the oxygen consumption curves show three distinct stages typical of bacterial growth: initial lag, followed by exponential growth, and ultimately, a stationary phase. First, S. oneidensis MR-1 cultures were exposed to 5 mg/L of all NMC morphologies. 5 mg/L was previously determined to be an impactful dose of NMC nanosheets to S. oneidensis MR-1.16 However, at a 5 mg/L dose, the respirometry data in Fig. 4a and 4b do not show a difference in toxicity between nanoblocks and commercial NMC. At a higher dose of 50 mg/L (Fig. 4c, 4d) a significant difference is observed, with the nanosheets resulting in complete cessation of detectable respiration. While these data show that the three different NMC materials elicit different biological responses, they do not establish whether the differences arise from intrinsic differences in the materials (for example, due to differences in the exposed crystal planes and degrees of structural disorder) or if they arise from other factors.

To explore these differences, we used the growth-based viability (GBV) assay. Compared to respirometry (Fig.4), the GBV assay provides higher throughput and thereby allows comparison of a larger number of samples over a wider range of dosing concentrations. Figure 5a shows that when using the GBV assay, the nanosheets, nanoblocks, and commercial NMC have significantly different toxicities (paired t-test, p<0.001) when doses are reported on a mass-based concentration basis. Since we measured the specific surface area of each material (exposed

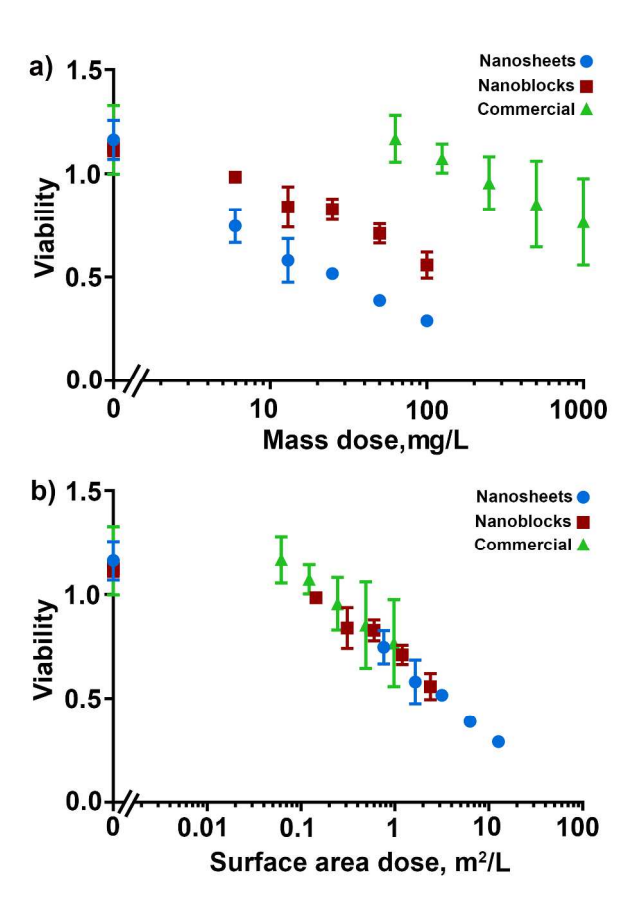


Figure 5. Viability in relation to (top) mass of dose per liter and (bottom) surface area of dose per liter. Error bars represent standard deviation.

surface area per unit mass) via the BET method, the mass-based concentration data in Fig. 5a can be renormalized to a graph of viability vs. the exposed surface area of NMC per unit volume of solution, yielding the graph in Fig. 5b. Importantly, when the data are replotted in this manner, all three NMC materials investigated collapse on a single dose-response curve. This collapse onto a single curve shows that the exposed surface area is the key factor in toxicity of these materials to *S. oneidensis* MR-1.

4. Discussion

The above experiments lead to several important observations. Our most important conclusion is that the ion release and subsequent toxicity of NMC materials toward *S. oneidensis* MR-1 do not depend strongly on the distribution of exposed crystal planes or degree of crystallinity, but can be accounted for almost entirely on the basis of differences in surface area. Secondly, we find that both nanosheet and nanoblock morphologies, as well as the commercially available material, release metals in an incongruent manner, with release in the order: Li>Ni>Co>Mn, regardless of any difference in presented crystal faces.

We also observed this ordering of release rates in a previous study of NMC materials with different stoichiometries.⁵⁻⁶ Our results show that while different processing methods produce nanomaterials with significantly different morphologies and associated distribution of crystal planes, these differences do not impact the detailed mechanism and/or rates of ion release (and associated toxicity) when normalized to constant surface area. This implies that the rates of ion release

from edge and basal planes are similar, despite likely differences in detailed chemical bonding.

4.1 Role of morphology and structural disorder. NMC materials can form several crystal structures. Prior studies have shown that NMC in the LiNi_{0.33}Mn_{0.33}Co_{0.33} O₂ stoichiometry studied here crystallizes in the delafossite (α -CuFeO₂) structure.⁵⁴ In NMC materials, the structure consists of layers of composition MO₂ (where M=a metal) separated by layers of Li⁺ ions. While detailed studies of the thermodynamics of NMC oxides have not been performed, prior studies of LiCoO₂ have shown that under oxidizing conditions, the (001) crystal face of $LiCoO_2$ is the most energetically favored, leading to formation of thin plates bounded by (104) and (012) planes at the edges.^{34, 55} As the lithium chemical potential is increased, the morphology favors the (104) and (012) planes, leading to changes in shape from the sheet-like structures to crystals that are prismatic in shape, elongated along the (001) direction.¹⁹ In prior studies, we have shown that under low-temperature growth, LiCoO₂ and NMC materials adopt very similar morphologies, consisting of flat plates with slightly hexagonal edges. Here, we extend that to show that annealing these materials in excess lithium transforms the nanoparticles into block-like structures. These transformations closely resemble those reported previously.^{19, 55-56} Our block-like structures are consistent with particles dominated by exposed (104) and (012) planes, as depicted in Fig. 1.

With NMC materials, a second consideration is the presence of disorder, and particularly cation exchange, wherein Ni²⁺ ions occupy sites normally occupied by Li⁺. ⁵⁷⁻⁵⁸ Modest amounts of cation mixing lead to a decrease in the intensity of the

(003) reflection compared to the (104) reflection. 52-53 Larger amounts of intermixing can lead to a new phase, referred to as the O1 phase, with reduced symmetry of $P\bar{3}m1$. This O1 phase has a distinctive diffraction pattern in which the most pronounced peaks are a (001) reflection at diffraction angle of 2θ =20 degrees and a (011) reflection at $2\theta = 42$ degrees (using CuK α radiation, as we do here). Examination of our XRD patterns in Figure 2 do not show any evidence for the O1 or any other phases. However, in addition to overall broadening of the pattern, we do observe that the (003) reflection is weaker than the (104) reflection; this indicates that there is indeed some cation mixing in the low-temperature nanosheets, and that the nanoblocks have a higher degree of structural order compared to the nanosheets. A Scherrer analysis comparing the width of the experimental and calculated diffraction patterns ⁴⁹ shows that the broadening observed for the nanoblocks is consistent with the sizes observed in TEM with an average diameter of approximately 25 nm; however, the nanosheets appears to have higher disorder than can be accounted for based on estimated thicknesses of ~ 10 nm.

4.2 Dissolution processes in aqueous media. While the (001) plane exposed for nanosheets is lower in energy than the (104) and (012) planes exhibited by nanoblocks, the chemical stability in aqueous media is expected to also be strongly modified by adsorption of H+, Li+, and/or OH- to the surface. Prior studies have shown that the dissolution behavior of metal oxides in aqueous media is typically controlled by successive adsorption of multiple H+ ions to the surface-exposed oxygens, forming a sequence of M(OH)_x surface intermediates that ultimately are released the surface. Stumm and co-workers³⁶ found that dissolution rates of

different metal oxide minerals scaled with the surface area (in agreement with our observations) and that they exhibited a strong correlation with the energy needed to break the M-O bonds.³⁶ Thermodynamic measurements of NMC-type metal oxides have shown that the enthalpies of formation of LiMnO₂, LiCoO₂, and LiNiO₂ from the elements are approximately -840, -678, and -593 kJ/mole.^{53,59} Mixed compositions were shown to behave like ideal solutions, having overall enthalpies close to those expected from the mole fraction of the individual metals.⁵² The thermodynamic ordering of the enthalpies of formation suggests that in mixedcomposition NMC materials, breaking of Ni-O bonds is expected to be more favorable than those of Co or Mn, in agreement with our observations of incongruent dissolution. More recent density functional calculations show that dissolution kinetics from the basal plane of LiCoO₂ is coupled with delithiation processes, 60 demonstrating that the simple protonation models used for simple binary metal oxides must be modified to properly account for dissolution kinetics of more complex oxides such as the NMC materials.

Based on the above analyses, we expected that the release rate, normalized to unit area, of the block-like structures would be higher than that of the nanosheets, since the nanosheets expose predominantly the (001) face, which has all transition metals coordinatively saturated. In contrast, we find that the area-normalized dissolution rate and associated metal toxicity of NMC nanomaterials does not vary strongly with crystal morphology or exposed crystal face. Similar response is measured when using a commercial NMC material as well. This uniformity of reaction rate may suggest that initial protonation events to form, -M(OH) or $-M(OH)_2$ species may be

much faster than formation of subsequent $-M(OH)_3$ and/or other labile species. In this case, the initial coordination of the metal exposed at the surface would have only minimal impact on the net dissolution rate, and hence, the coordination of the initial surface species would not be a factor in the rate-limiting step.

Delineating a detailed kinetic model for dissolution of NMC nanomaterials is complicated by the fact that dissolution of these high-valence oxides couples acid-base chemistry with oxidation-reduction chemistry. The oxidation states of transition metal ions in LiNi_{1/3}Mn_{1/3}Co _{1/3}O₂ are Li⁺, Ni²⁺, Mn⁴⁺, and Co³⁺. Because Co³⁺ is not thermodynamically stable in water,⁶¹ "dissolution" of NMC also likely involves oxidation of water, which is a kinetically hindered reaction. ¹² Release of Li⁺ is fast because H⁺ ions can rapidly exchange for Li⁺, while Ni²⁺ release is the most thermodynamically favorable.^{6, 39} Subsequent steps to release Mn⁴⁺ and Co²⁺ or Co³⁺ require protonation of surface sites and removal of transition metal hydroxides. ³⁹ The detailed pathways and kinetic rates of these processes remain under investigation, and further studies will be needed to develop predictive kinetic models for dissolution of NMC and related complex oxides.

Prior studies of environmental toxicity have highlighted the need to understand what specific nanomaterial properties control their chemical and biological interactions. 1-4, 29-30, 32 In the context of NMC materials, our results suggest that, even though cycling of battery materials leads to the formation of new phases and both chemical and structural disorder, 57 the overall chemical processes that impact the release and subsequent toxicity are not strongly dependent on the structural details. This implies, for example, that cathode materials that have been cycled

many times (and therefore have a higher degree of structural disorder) are expected to have environmental and toxicological impact similar to pristine materials. Our work also indicates that as nanomaterials are increasingly incorporated into emerging battery technologies, it may be possible to predict the impact through simple size-dependent scaling of the specific surface area. In the case of the NMC class of nanomaterials, we find that the important properties are controlled by the nanomaterial surface area and that other factors such as distribution of specific crystal planes and/or presence of disorder does not significantly impact the overall chemical and biological impact of the materials.

We note that due to the wide variety or organisms in the environment, generalizing results to an overall assessment of environmental impact will ultimately require experiments using additional organisms. ⁴¹ Yet, because batteries and other forms of electronic waste are likely to end up in landfills, ²⁵⁻²⁷ soil bacteria such as *Shewanella oneidensis MR-1* are one of the organisms most likely to experience direct exposure to high concentrations of NMC nanomaterials after disposal. We conjecture that mechanisms of toxicity might be expected to exhibit some similarities within broad classes of organisms (e.g., Gram-negative bacteria), such that understanding the chemical factors that influence these mechanisms provides important molecular-level insights that may be useful in understanding broader environmental implications and also guiding future development of more benign nanomaterials. For example, since transition metal ion release is the dominant factor controlling toxicity toward *Shewanella*, the application of organic or inorganic coatings that slow down the kinetics of ion release may reduce toxicity. ³²

Indeed, within the battery industry very thin (nanometer-thickness) coatings of highly stable materials, typically insulating oxides such as such as Al₂O₃ or AlF₃ are sometimes applied to NMC cathode materials to reduce dissolution of transition metal ions into the non-aqueous solvents used in lithium-ion batteries. ⁶²⁻⁶⁴ To be effective without adversely affecting battery performance those coatings must be very thin (nanometers) in order to facilitate electrical conduction and Li⁺ diffusion and are frequently incomplete. Such thin coatings are frequently amorphous and often incomplete. As a result, it is likely that thin coatings will eventually dissolve in aqueous media. However, we conjecture that they might be able to mitigate adverse environmental impact in aqueous media by reducing the rate of dissolution and the resulting metal ion concentrations to levels that can be accommodated by natural defense mechanisms.

5. Conclusions

Our work provides new fundamental insights into the molecular-level factors that impact the environmental and biological impact of NMC nanomaterials. Morphology control represents one approach to altering the performance characteristics of lithium intercalation materials when used in applications in energy storage ³⁴ and catalysis. ¹² In energy storage, the total energy that can be stored in lithium intercalation materials is controlled by the particle mass, while the rate at which energy can be stored and released is controlled by the morphology because lithium intercalation can only occur through edge-plane sites. However, the edge planes have higher energy, suggesting greater reactivity. Our results show that altering the

morphology to increase the fractional surface area consisting of these edge planes does not by itself increase the overall rate of metal release or biological impact of NMC nanomaterials. Rather, our studies show that the rate of metal release and the subsequent biological impact are controlled primarily by the total surface area that is exposed. This conclusion holds both for synthesized nanomaterials and commercially available NMC. Since release of TMs into aqueous media involves breaking multiple surface bonds, our work implies that the critical steps controlling the rate of metal release and resulting biological impact are not dominated by the different coordination of the initial basal and/or edge plane sites, but are controlled by later steps. This suggests that it should be feasible to predict the environmental impact of NMC and related nanomaterials of different sizes and morphology using the total exposed surface areas as the primary dosing metric.²⁹⁻³⁰

Associated Content

Supporting Information

The Supporting Information is available free of charge on the ACS Publications website at DOI: 10.10201/acsanm.xxxxxx

Additional SEM images characterizing changes in morphology of NMC as a function of different synthesis variables. Additional dissolution data including Li⁺ ion controls for respirometry data.

Author Information

Corresponding Author

*E-mail: <u>rjhamers@wisc.edu</u>

ORCID

Dr. Robert J. Hamers: 0000-0003-3821-9625

Dr. Christy L. Haynes: 0000-0002-5420-5867

Natalie V. Hudson-Smith: 0000-0002-2642-0711

Peter L. Clement: 0000-0003-2959-7253

Notes

The authors declare no competing financial interest.

Acknowledgments

This work was supported by the National Science Foundation Centers for Chemical Innovation Program, Grant CHE-1503408 to the Center for Sustainable Nanotechnology. MNH and NVH acknowledge support through the National Science Foundation Graduate Research Fellowship Program. NVH also acknowledges partial support through the NIH Biotechnology Training Grant under No. T32 GM 8347.

References

- (1) Garner, K. L.; Suh, S.; Keller, A. A. Assessing the Risk of Engineered Nanomaterials in the Environment: Development and Application of the Nanofate Model. *Environ. Sci. Technol.* **2017**, *51*, 5541-5551.
- (2) Gardea-Torresdey, J. L.; Rico, C. M.; White, J. C. Trophic Transfer, Transformation, and Impact of Engineered Nanomaterials in Terrestrial Environments. *Environ. Sci. Technol.* **2014**, *48*, 2526-2540.

- (3) Nowack, B.; Ranville, J. F.; Diamond, S.; Gallego-Urrea, J. A.; Metcalfe, C.; Rose, J.; Horne, N.; Koelmans, A. A.; Klaine, S. J. Potential Scenarios for Nanomaterial Release and Subsequent Alteration in the Environment. *Environ. Toxicol. Chem.* **2012**, *31*, 50-59.
- (4) Wang, Z.; von dem Bussche, A.; Kabadi, P. K.; Kane, A. B.; Hurt, R. H. Biological and Environmental Transformations of Copper-Based Nanomaterials. *ACS Nano* **2013**, *7*, 8715-8727.
- (5) Hang, M. N.; Gunsolus, I. L.; Wayland, H.; Melby, E. S.; Mensch, A. C.; Hurley, K. R.; Pedersen, J. A.; Haynes, C. L.; Hamers, R. J. Impact of Nanoscale Lithium Nickel Manganese Cobalt Oxide (Nmc) on the Bacterium *Shewanella oneidensis* MM-1. *Chem. Mat.* **2016**, *28*, 1092-1100.
- (6) Gunsolus, I. L.; Hang, M. N.; Hudson-Smith, N. V.; Buchman, J. T.; Bennett, J. W.; Conroy, D.; Mason, S. E.; Hamers, R. J.; Haynes, C. L. Influence of Nickel Manganese Cobalt Oxide Nanoparticle Composition on Toxicity toward *Shewanella oneidensis* MR-1: Redesigning for Reduced Biological Impact. *Environ. Sci.: Nano* **2017**, *4*, 636-646.
- (7) Bruce, P. G.; Scrosati, B.; Tarascon, J. M. Nanomaterials for Rechargeable Lithium Batteries. *Angew. Chem. Int. Edit.* **2008**, *47*, 2930-2946.
- (8) Winter, M.; Besenhard, J. O.; Spahr, M. E.; Novak, P. Insertion Electrode Materials for Rechargeable Lithium Batteries. *Adv. Mater.* **1998**, *10*, 725-763.
- (9) Van der Ven, A.; Aydinol, M. K.; Ceder, G.; Kresse, G.; Hafner, J. First-Principles Investigation of Phase Stability in Li_xCoO₂. *Phys. Rev. B* **1998**, *58*, 2975-2987.

- (10) Mizushima, K.; Jones, P. C.; Wiseman, P. J.; Goodenough, J. B. Li_xCoO_2 (x<1) a New Cathode Material for Batteries of High Energy Density *Mater. Res. Bull.* **1980**, *15*, 783-789.
- (11) Bajdich, M.; Garcia-Mota, M.; Vojvodic, A.; Norskov, J. K.; Bell, A. T. Theoretical Investigation of the Activity of Cobalt Oxides for the Electrochemical Oxidation of Water. *J. Am. Chem. Soc.* **2013**, *135*, 13521-13530.
- (12) Lu, Z. Y.; Chen, G. X.; Li, Y. B.; Wang, H. T.; Xie, J.; Liao, L.; Liu, C.; Liu, Y. Y.; Wu, T.; Li, Y. Z.; Luntz, A. C.; Bajdich, M.; Cui, Y. Identifying the Active Surfaces of Electrochemically Tuned LiCoO₂ for Oxygen Evolution Reaction. *J. Am. Chem. Soc.* **2017**, *139*, 6270-6276.
- (13) Liu, H. F.; Zhou, Y.; More, R.; Muller, R.; Fox, T.; Patzke, G. R. Correlations among Structure, Electronic Properties, and Photochemical Water Oxidation: A Case Study on Lithium Cobalt Oxides. *ACS Catal.* **2015**, *5*, 3791-3800.
- (14) Lu, Z. H.; MacNeil, D. D.; Dahn, J. R. Layered LiNi_xCo_{1-2x}Mn_xO₂ Cathode Materials for Lithium-Ion Batteries. *Electrochem. Solid State Lett.* **2001**, *4*, A200-A203.
- (15) Tarascon, J. M.; Armand, M. Issues and Challenges Facing Rechargeable Lithium Batteries. *Nature* **2001**, *414*, 359-367.
- (16) Yabuuchi, N.; Ohzuku, T. Novel Lithium Insertion Material of $\label{eq:LiCo1/3} \text{LiCo}_{1/3} \text{Ni}_{1/3} \text{Mn}_{1/3} \text{O}_2 \text{ for Advanced Lithium-Ion Batteries.} \textit{J. Power Sources 2003, 119,} \\ 171-174.$
- (17) Liu, L.; Tian, F. H.; Wang, X. Y.; Yang, Z. H.; Chen, Q. Q.; Wang, X. Y. Electrochemical Behavior of Spherical $LiNi_{1/3}Co_{1/3}Mn_{1/3}O_2$ as Cathode Material for

Aqueous Rechargeable Lithium Batteries. *J. Solid State Electrochem.* **2012**, *16*, 491-497.

- (18) Ates, M. N.; Jia, Q. Y.; Shah, A.; Busnaina, A.; Mukerjee, S.; Abraham, K. M. Mitigation of Layered to Spinel Conversion of a Li-Rich Layered Metal Oxide Cathode Material for Li-Ion Batteries. *J. Electrochem. Soc.* **2014**, *161*, A290-A301.
- (19) Garcia, J. C.; Bareno, J.; Yan, J. H.; Chen, G. Y.; Hauser, A.; Croy, J. R.; Iddir, H. Surface Structure, Morphology, and Stability of Li(Ni_{1/3}Mn_{1/3} Co_{1/3})O₂ Cathode Material. *J. Phys. Chem. C* **2017**, *121*, 8290-8299.
- (20) Chen-Wiegart, Y. C. K.; Liu, Z.; Faber, K. T.; Barnett, S. A.; Wang, J. 3d Analysis of a LiCoO₂ Li(Ni_{1/3}Mn_{1/3} Co_{1/3})O₂ Li-Ion Battery Positive Electrode Using X-Ray Nano-Tomography. *Electrochem. Comm.* **2013**, *28*, 127-130.
- (21) Cheng, Q.; Yang, T.; Li, M.; Chan, C. K. Exfoliation of LiNi_{1/3}Mn_{1/3} Co_{1/3}O₂ into Nanosheets Using Electrochemical Oxidation and Reassembly with Dialysis or Flocculation. *Langmuir* **2017**, *33*, 9271-9279.
- (22) Zhao, Y. L.; Han, C. H.; Yang, J. W.; Su, J.; Xu, X. M.; Li, S.; Xu, L.; Fang, R. P.; Jiang, H.; Zou, X. D.; Song, B.; Mai, L. Q.; Zhang, Q. J. Stable Alkali Metal Ion Intercalation Compounds as Optimized Metal Oxide Nanowire Cathodes for Lithium Batteries.

 Nano Lett. 2015, 15, 2180-2185.
- (23) Bazito, F. F. C.; Torresi, R. M. Cathodes for Lithium Ion Batteries: The Benefits of Using Nanostructured Materials. *J. Braz. Chem. Soc.* **2006**, *17*, 627-642.
- (24) Kumar, P.; Kim, K. H.; Bansal, V.; Kumar, P. Nanostructured Materials: A Progressive Assessment and Future Direction for Energy Device Applications. *Coord. Chem. Rev.* **2017**, *353*, 113-141.

- (25) Gu, F.; Guo, J. F.; Yao, X.; Summers, P. A.; Widijatmoko, S. D.; Hall, P. An Investigation of the Current Status of Recycling Spent Lithium-Ion Batteries from Consumer Electronics in China. *J. Clean Prod.* **2017**, *161*, 765-780.
- (26) Diekmann, J.; Hanisch, C.; Frobose, L.; Schalicke, G.; Loellhoeffel, T.; Folster, A. S.; Kwade, A. Ecological Recycling of Lithium-Ion Batteries from Electric Vehicles with Focus on Mechanical Processes. *J. Electrochem. Soc.* **2017**, *164*, A6184-A6191.
- (27) Zeng, X. L.; Li, J. H.; Liu, L. L. Solving Spent Lithium-Ion Battery Problems in China: Opportunities and Challenges. *Renew. Sust. Energ. Rev.* **2015**, *52*, 1759-1767.
- (28) Dunn, J. B.; Gaines, L.; Kelly, J. C.; James, C.; Gallagher, K. G. The Significance of Li-Ion Batteries in Electric Vehicle Life-Cycle Energy and Emissions and Recycling's Role in Its Reduction. *Energy Environ. Sci.* **2015**, *8*, 158-168.
- (29) Unrine, J. M.; Tsyusko, O. V.; Hunyadi, S. E.; Judy, J. D.; Bertsch, P. M. Effects of Particle Size on Chemical Speciation and Bioavailability of Copper to Earthworms (Eisenia Fetida) Exposed to Copper Nanoparticles. *J. Environ. Qual.* **2010**, *39*, 1942-1953.
- (30) Lowry, G. V.; Hotze, E. M.; Bernhardt, E. S.; Dionysiou, D. D.; Pedersen, J. A.; Wiesner, M. R.; Xing, B. S. Environmental Occurrences, Behavior, Fate, and Ecological Effects of Nanomaterials: An Introduction to the Special Series. *J. Environ. Qual.* **2010**, *39*, 1867-1874.
- (31) von der Kammer, F.; Ferguson, P. L.; Holden, P. A.; Masion, A.; Rogers, K. R.; Klaine, S. J.; Koelmans, A. A.; Horne, N.; Unrine, J. M. Analysis of Engineered Nanomaterials in Complex Matrices (Environment and Biota): General

Considerations and Conceptual Case Studies. *Environ. Toxicol. Chem.* **2012,** *31,* 32-49.

- (32) Suresh, A. K.; Pelletier, D. A.; Doktycz, M. J. Relating Nanomaterial Properties and Microbial Toxicity. *Nanoscale* **2013**, *5*, 463-474.
- (33) Wu, E. J.; Tepesch, P. D.; Ceder, G. Size and Charge Effects on the Structural Stability of Limo2 (M = Transition Metal) Compounds. *Philos. Mag. B.* **1998**, *77*, 1039-1047.
- (34) Kramer, D.; Ceder, G. Tailoring the Morphology of LiCoO₂: A First Principles Study. *Chem. Mat.* **2009**, *21*, 3799-3809.
- (35) Trovarelli, A.; Llorca, J. Ceria Catalysts at Nanoscale: How Do Crystal Shapes Shape Catalysis? *ACS Catal.* **2017**, *7*, 4716-4735.
- (36) Wieland, E.; Wehrli, B.; Stumm, W. The Coordination Chemistry of Weathering. 3. A Generalization on the Dissolution Rates of Minerals. *Geochim. Cosmochim. Acta* **1988**, *52*, 1969-1981.
- (37) Stumm, W.; Wollast, R. Coordination Chemistry of Weather Kinetics of the Surface-Controlled Dissolution of Oxide Minerals. . *Rev. Geophys.* **1990**, *28*, 53-69. (38) Stumm, W., *Chemistry of the Solid-Water Interface*. John Wiley & Sons: New
- York, **1992**.
- (39) Bennett, J. W.; Jones, D.; Huang, X.; Hamers, R. J.; Mason, S. E. Dissolution of Complex Metal Oxides from First-Principles and Thermodynamics: Cation Removal from the (001) Surface of Li(Ni_{1/3}Mn_{1/3} Co_{1/3})O₂. *Environ. Sci. Technol.* **2018**, *submitted for publication*.

- (40) Beliaev, A. S.; Klingeman, D. M.; Klappenbach, J. A.; Wu, L.; Romine, M. F.; Tiedje, J. M.; Nealson, K. H.; Fredrickson, J. K.; Zhou, J. Global Transcriptome Analysis of Shewanella Oneidensis Mr-1 Exposed to Different Terminal Electron Acceptors. *J. Bacteriol.* **2005**, *187*, 7138-7145.
- (41) Kenaga, E. E. Test Organisms and Methods Useful for Early Assessment of Acute Toxicity of Chemicals. *Environ. Sci. Technol.* **1978,** *12*, 1322-1329.
- (42) Blaylock, B. G.; Frank, M. L.; McCarthy, J. F. Comparative Toxicity of Copper and Acridine to Fish, Daphnia and Algae. *Environ. Toxicol. Chem.* **1985**, *4*, 63-71.
- (43) Suresh, A. K.; Pelletier, D. A.; Wang, W.; Moon, J. W.; Gu, B. H.; Mortensen, N. P.; Allison, D. P.; Joy, D. C.; Phelps, T. J.; Doktycz, M. J. Silver Nanocrystallites: Biofabrication Using Shewanella Oneidensis, and an Evaluation of Their Comparative Toxicity on Gram-Negative and Gram-Positive Bacteria. *Environ. Sci. Technol.* **2010**, *44*, 5210-5215.
- (44) Pelletier, D. A.; Suresh, A. K.; Holton, G. A.; McKeown, C. K.; Wang, W.; Gu, B. H.; Mortensen, N. P.; Allison, D. P.; Joy, D. C.; Allison, M. R.; Brown, S. D.; Phelps, T. J.; Doktycz, M. J. Effects of Engineered Cerium Oxide Nanoparticles on Bacterial Growth and Viability. *Appl. Environ. Microbiol.* **2010**, *76*, 7981-7989.
- (45) Toes, A. C. M.; Daleke, M. H.; Kuenen, J. G.; Muyzer, G. Expression of Copa and Cusa in Shewanella During Copper Stress. *Microbiology-(UK)* **2008**, *154*, 2709-2718.
- (46) Buchman, J. T.; Rahnamoun, A.; Landy, K. M.; Zhang, X.; Vartanian, A. M.; Jacob, L. M.; Murphy, C. J.; Hernandez, R.; Haynes, C. L. Using an Environmentally-Relevant Panel of Gram-Negative Bacteria to Assess the Toxicity of Polyallylamine Hydrochloride-Wrapped Gold Nanoparticles. *Environ.-Sci. Nano* **2018**, *5*, 279-288.

- (47) Bozich, J.; Hang, M.; Hamers, R.; Klaper, R. Core Chemistry Influences the Toxicity of Multicomponent Metal Oxide Nanomaterials, Lithium Nickel Manganese Cobalt Oxide, and Lithium Cobalt Oxide to Daphnia Magna. *Environ. Toxicol. Chem.* **2017**, *36*, 2493-2502.
- (48) Qiu, T. A.; Nguyen, T. H. T.; Hudson-Smith, N. V.; Clement, P. L.; Forester, D. C.; Frew, H.; Hang, M. N.; Murphy, C. J.; Hamers, R. J.; Feng, Z. V.; Haynes, C. L. Growth-Based Bacterial Viability Assay for Interference -Free and High-Throughput Toxicity Screening of Nanomaterials. *Anal. Chem.* **2017**, *89*, 2057-2064.
- (49) Yin, S. C.; Rho, Y. H.; Swainson, I.; Nazar, L. F. X-Ray/Neutron Diffraction and Electrochemical Studies of Lithium De/Re-Intercalation in Li_{1-X}Ni_{1/3}Mn_{1/3} Co_{1/3}O₂ (x<1). *Chem. Mat.* **2006**, *18*, 1901-1910.
 - (50) CrystalDiffract; CrystalMaker LTD, Pembroke, Oxfordshire, UK. .
- (51) Okubo, M.; Hosono, E.; Kim, J.; Enomoto, M.; Kojima, N.; Kudo, T.; Zhou, H. S.; Honma, I. Nanosize Effect on High-Rate Li-Ion Intercalation in LiCoO₂ Electrode. *J. Am. Chem. Soc.* **2007**, *129*, 7444-7452.
- (52) Masoumi, M.; Cupid, D. M.; Reichmann, T. L.; Chang, K. K.; Music, D.; Schneider, J. M.; Seifert, H. J. Enthalpies of Formation of Layered LiNi $_x$ Mn $_x$ Co $_{1-2x}$ O $_2$ ($0 \le x \le 0.5$) Compounds as Lithium Ion Battery Cathode Materials. *Int. J. Mater. Res.* **2017**, *108*, 869-878.
- (53) Wang, M. J.; Navrotsky, A. Li MO_2 (M = Mn, Fe, and Co): Energetics, Polymorphism and Phase Transformation. *J. Solid State Chem.* **2005**, *178*, 1230-1240.

- (54) Sencanski, J.; Bajuk-Bogdanovic, D.; Majstorovic, D.; Tchernychova, E.; Papan, J.; Vujkovic, M. The Synthesis of Li(Co-Mn-Ni)O₂ Cathode Material from Spent-Li Ion Batteries and the Proof of Its Functionality in Aqueous Lithium and Sodium Electrolytic Solutions. *J. Power Sources* **2017**, *342*, 690-703.
- (55) Chen, H. L.; Grey, C. P. Molten Salt Synthesis and High Rate Performance of the "Desert-Rose" Form of Licoo2. *Adv. Mater.* **2008,** *20*, 2206-2210.
- (56) Sharifi-Asl, S.; Soto, F. A.; Nie, A. M.; Yuan, Y. F.; Asayesh-Ardakani, H.; Foroozan, T.; Yurkiv, V.; Song, B.; Mashayek, F.; Klie, R. F.; Amine, K.; Lu, J.; Balbuena, P. B.; Shahbazian-Yassar, R. Facet-Dependent Thermal Instability in LiCoO₂. *Nano Lett.* **2017**, *17*, 2165-2171.
- (57) Reynaud, M.; Casas-Cabanas, M. Order and Disorder in NMC Layered Materials: A Faults Simulation Analysis. *Powder Diffr.* **2017**, *32*, S213-S220.
- (58) Zhang, X. Y.; Jiang, W. J.; Mauger, A.; Qilu; Gendron, F.; Julien, C. M. Minimization of the Cation Mixing in $\text{Li}_{1-x}(\text{NMC})_{(1-x)}O_2$ as Cathode Material. *J. Power Sources* **2010**, *195*, 1292-1301.
- (59) Wang, M.; Navrotsky, A. Enthalpy of Formation of LiNiO₂, LiCoO₂ and Their Solid Solution, LiNi_{1-X}Co_xO₂. *Solid State Ionics* **2004**, *166*, 167-173.
- (60) Huang, X.; Bennett, J. W.; Hang, M. M. N.; Laudadio, E. D.; Hamers, R. J.; Mason, S. E. Ab Initio Atomistic Thermodynamics Study of the (001) Surface of LiCoO₂ in a Water Environment and Implications for Reactivity under Ambient Conditions. *J. Phys. Chem. C* **2017**, *121*, 5069-5080.
- (61) Vanysek, P., Electrochemical Series. In *CRC Handbook of Chemistry and Physics*, 92nd ed.; CRC Press.

- (62) Kim, J. W.; Travis, J. J.; Hu, E. Y.; Nam, K. W.; Kim, S. C.; Kang, C. S.; Woo, J. H.; Yang, X. Q.; George, S. M.; Oh, K. H.; Cho, S. J.; Lee, S. H. Unexpected High Power Performance of Atomic Layer Deposition Coated LiNi_{1/3}Mn_{1/3}Co_{1/3}O₂ Cathodes. *J. Power Sources* **2014**, *254*, 190-197.
- (63) Jackson, D. H. K.; Laskar, M. R.; Fang, S. Y.; Xu, S. Z.; Ellis, R. G.; Li, X. Q.; Dreibelbis, M.; Babcock, S. E.; Mahanthappa, M. K.; Morgan, D.; Hamers, R. J.; Kuech, T. F. Optimizing Alf3 Atomic Layer Deposition Using Trimethylaluminum and TaF₅: Application to High Voltage Li-Ion Battery Cathodes. *J. Vac. Sci. Technol. A* **2016**, *34*, 8.
- (64) Han, B. H.; Paulauskas, T.; Key, B.; Peebles, C.; Park, J. S.; Klie, R. F.; Vaughey, J. T.; Dogan, F. Understanding the Role of Temperature and Cathode Composition on Interface and Bulk: Optimizing Aluminum Oxide Coatings for Li-Ion Cathodes. *ACS Appl. Mater. Interfac.* **2017**, *9*, 14769-14778.

Table-of-contents Graphic:

